

# The gold quartz vein of Pontal, Tocantins, Brazil

Moacyr Martins dos Santos - *Metais de Goiás S.A., Goiânia, GO, Brazil*

Gaston Giuliani - *Instituto de Geociências, Universidade de Brasília, Brazil & ORSTOM / CRPG, Nancy, France*

Jean C. Touray - *ESEM, Université de Orléans, France*

Marcel August Dardenne - *Instituto de Geociências, Universidade de Brasília, D.F., Brazil*

Nicole Guilhaumou - *Département de Géologie, ENS, Paris, France*

Clair Beny - *Gis BRGM, CNRS, Orléans, France*

**ABSTRACT:** The Pontal deposit consists of an auriferous quartz vein hosted by tonalitic orthogneisses deformed by ductil shear and metamorphosed in the amphibolite facies. It is generally concordant with the mylonitic foliation of surrounding gneisses, presenting a tabular aspect and boudinaged structure. Its mineral assemblage consists of oligoclase, actinolite, biotite and less 2% sulfides (pyrrhotite, pyrite, sphalerite, chalcopryrite and galena). Native gold occurs as disseminated particles in the quartz crystal interstices or sometimes filling fractures. Primary inclusions present in the quartz matrix are geometrically related to gold particles, and contain a  $H_2O-CH_4$  fluid, daughter and trapped solids (graphite, siderite, dolomite, calcite, biotite, actinolite and rutile). Trapping temperature range from 300 to 420°C. The presence of graphite and carbonates lead to the supposition that gold deposition has occurred in a reducing system at elevated temperature with boundary conditions between greenschist and amphibolite facies, related to decreases of oxygen fugacity and pH.

## 1 INTRODUCTION

The Pontal deposit is located in the Tocantins state, Brazil, at the latitude 10°52' and latitude 48°36' (figure 1).

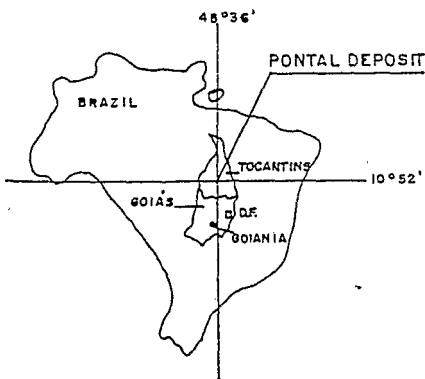


Fig. 1 Localization

Presently, 10,000 tons of auriferous quartz vein with an average grade of about 17,5 ppm Au have been mined by Metago.

The mineralization formed before 1.8 b.y. and presumably during early Proterozoic ti-

mes. It occurred after the metamorphism of the host basement rocks to the amphibolite facies.

Petrological interpretation of the mineral association trapped in quartz as solid inclusions as well as a study of its fluid inclusions (microthermometry and Raman analyses) have been done to establish the physico-chemical conditions prevailing during ore deposition.

## 2 REGIONAL GEOLOGY

Geophysical data (gravimetry and magnetometry) deduced a structural framework for Goiás and Tocantins states, linked through thrust zones in four crustal blocks named Araguacema, Porangatu, Brasília and Paraná (Hasui et al., 1985; figure 2).

The Pontal deposit is hosted by archaean gneisses of Goiás basement complex (figure 3) located at the northeastern part of Porangatu block which overthrust the Araguacema block and are overthrust by the Brasília block. This block is intersected by regional lineaments with NNE strike (Transbrasilian lineaments; Schobbenhaus, 1975) represented by faults and transcurrent ductil shear zones with isochronous Rb-Sr age about 2.0 b.y. (Costa et al., 1988).

589 R.S.T.O.M. Fonds Documentaire

N° : 34.850 ex-1

Cpte : B

23 OCT. 1991

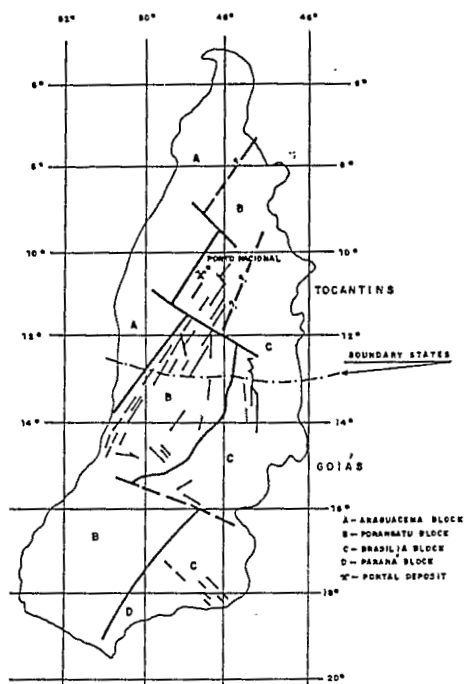


Fig. 2 Structural framework for Goiás and Tocantins states

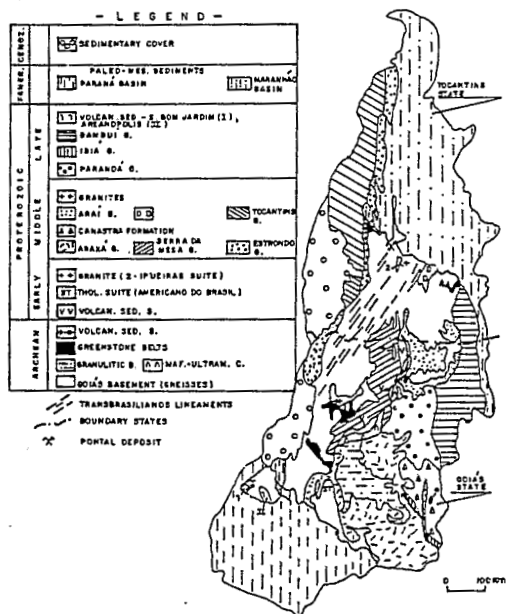


Fig. 3 Simplified geology of Goiás and Tocantins states

### 3 LOCAL GEOLOGY

The main lithologic unit exposed in the mine area consists of biotitic and biotite-hornblende orthogneisses with amphibolite intercalations. The observed mineral association in these rocks (oligoclase+quartz+biotite+hornblende+garnet) are diagnostic for metamorphic culmination in the amphibolite facies. The orthogneisses display a mylonitic foliation oriented N15-30E and dipping 60 to 70°SE. A subhorizontal stretching lineation defined by oriented biotite platelets and various deformation aspects as anastomosed foliation, rotationed sigmoidal, sheet folds and boudinage, suggests a transcurrent ductile deformation in a dextral simple shear regime.

Auriferous saccharoidal quartz veins white to dark grey coloured are usually parallel to the mylonitic gneisses foliation and sometimes cut it at low angle. They have variable length (centimetric to decametric) with maximum of 120m (Pontal deposit). Barren quartz veins, milk coloured and fine grained, cut either mylonitic gneisses or saccharoidal veins at high angle.

Later granitic intrusions (porphyritic biotite granite and fine biotite granite) contain xenolites of mylonitic gneisses and have related pegmatitic injections that cut both metamorphic basement and quartz veins. Porphyritic biotite granite belongs to Ipueiras suite, and presents Rb-Sr isochronous age about 1,8 b.y. (Costa et al., 1988).

Devonian detrital sediments of Pimenteira Formation (rhythmic alternation of ferruginous arenite, siltstone and argillite) overlay the basement and granitic rocks unconformably (figure 4).

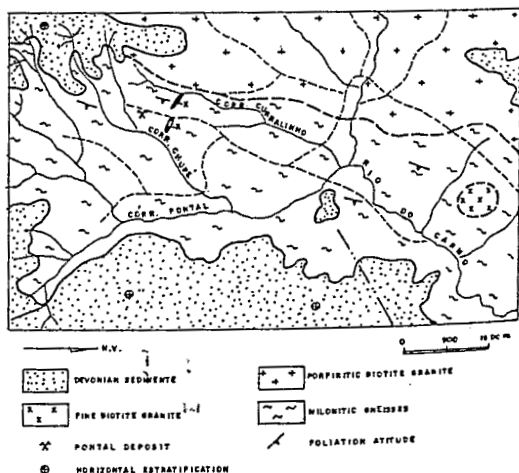


Fig. 4 Geology of mine area

## 4 MINERALIZATION CHARACTERISTICS

The auriferous quartz vein at the Pontal deposit presents a tabular aspect: 120m along strike, 0.5m average thickness and 60 to 100m down dip. It is concordant with the mylonitic gneisses (N15-30E, 60-70SE) and sometimes cuts it at a low angle. This lens is boudinaged (centimetric to metric) parallel to the X axis of strain ellipsoid (figure 5).

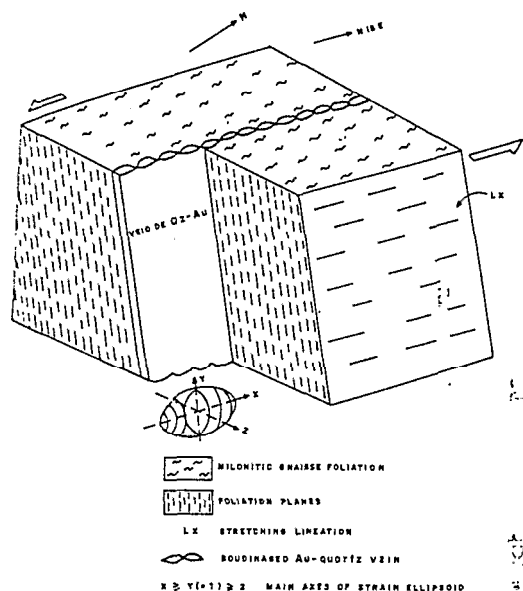


Fig. 5 Schematic diagram block of deformation at the mine area

Its mineralogical assemblage is dominantly composed of white to dark grey saccharoidal quartz (90%) showing undulated extinction with indented and saturated contacts. The remainder are biotite (4%), oligoclase (3%), tremolite/actinolite (1%) and around 2% sulfides (55% pyrrhotite, 28% pyrite, 9% sphalerite, 6% chalcopryrite and 1% galena). Microprobe investigation of quartz revealed solid inclusions of actinolite/tremolite, oligoclase and biotite.

Native gold occurs as irregular and euhedral disseminated particles in the quartz crystal interstices or sometimes filling fractures, with sizes spanning in the following fractions: 25% over +65 mesh (0.21mm), 22% over +100 mesh (0.15mm), 29% over +200 mesh (0.074mm), 9% over +270 mesh (0.053mm) and 15% below +270 mesh. Only 3% and 2% gold are associated with sulfides and silicates respectively.

## 5 FLUID INCLUSIONS STUDIES

### 5.1 Typology

Five main types of fluid inclusions have been defined from microscopical observations:

Type 1 - large sized (about 15 to 80  $\mu$ m) multiphase primary inclusions, with low filling degree by the vapour phase (0.1 to 0.2). They are isolated within quartz grains and contain several solids with distinct shape, colour, refractive index and birefringence (foto 1).

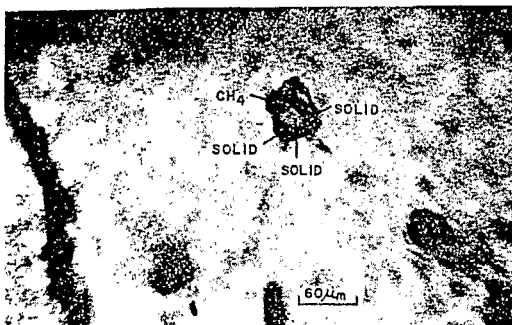


Foto 1 Type 1 multiphase fluid inclusion

Type 2 - are medium sized (about 10 to 40  $\mu$ m) triphase (L+V+S) pseudo-secondary and/or secondary inclusions with a filling degree by the vapour phase of about 0.3 to 0.4. They form groups within a same crystal or trail cross-cutting boundaries of quartz grains (foto 2).

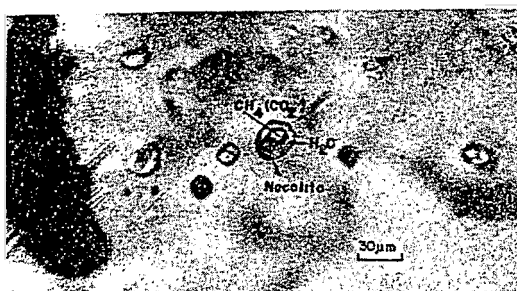


Foto 2 Type 2 triphase inclusion

Type 3 - are small to medium sized (about 3 to 40  $\mu$ m) two-phase (L+V) pseudo-secondary and/or secondary inclusions with a filling degree by the vapour phase of about

0.3 to 0.4. They form groups within a same crystal or trail cross-cutting boundaries of quartz grains (foto 3).



Foto 3 - Type 3 Two-phase pseudo-secondary and/or secondary inclusions

Type 4 - are small to medium sized (about 3 to 20 μm) two-phase (L+V) primary inclusions with a filling degree by vapour of about 0.9. They appear scattered within the quartz crystals (foto 4).

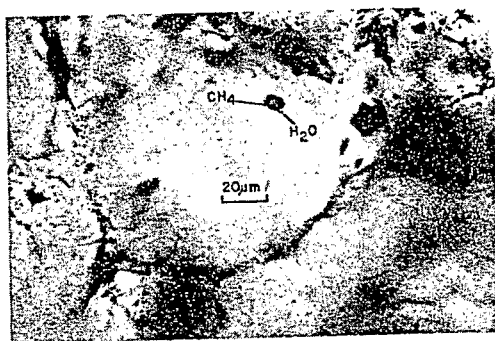


Foto 4 - Type 4 Two-phase primary inclusion

Type 5 - are small to large sized (about 3 to 50 μm) two-phase (L+V) secondary inclusions of late origin, with a filling degree by vapour of about 0.1 (foto 5).



Foto 5 Type 5 two-phase secondary inclusions

## 5.2 Raman microprobe data

Raman spectra of gas and solids on the main type inclusions have been established using a U 1000 apparatus (Guilhaumou et al., 1989).

Type 1 - contain trapped biotite and amphibole comparable with spectra from same phases trapped as isolated large sized solids inclusions in the quartz matrix. Also trapped appears rutile with characteristic peaks at 448 and 610  $\text{cm}^{-1}$  (figure 6).

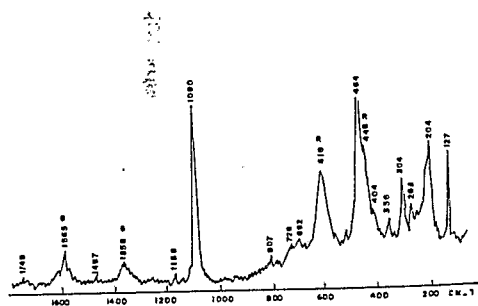


Fig. 6 Raman spectra of graphite and rutile

Daughter phases were determined as graphite-like grains identified by two broad bands at about 1360 and 1590  $\text{cm}^{-1}$  (figure 6), and rhomboedral carbonates represented by siderite, dolomite and calcite, as shown by characteristic peaks on Raman spectra (table 1). In vapour phase, mainly  $\text{CH}_4$  has been detected and several percents of  $\text{CO}_2$  (table 2).

Table 1. Raman spectra for carbonates

Reference	$2\nu_2$	$\nu\text{CO}_3$	$\nu_4$	L	T	Phases
N35110BIFC						
S1	1753	1094	722	295	170	dolomite
S2	1737	1091	733	300	192	siderite
N35110BIFA						
S1	1736	1809	735	302	196	siderite
N22AZIFA						
A35	1744	1091	735	105	193	siderite
N3580BIFD						
S1	--	1090	736	304	195	siderite
N3580BIFA						
S1	--	1092	730	306	197	siderite
N3580BIA						
S1	--	1092	736	306	193	siderite
N1101FA						
S1	--	1092	734	305	200	siderite
N156CA						
S1	--	1094	723	299	171	calcite
S2	--	1087	713	283	156	calcite

$2\nu_2$  - Out of plane bend  
 $\nu\text{CO}_3$  - Symmetric stretch of CO in  $\text{CO}_3$   
 $\nu_4$  - In plane bend  
L - Libration mode  
T - Translation mode

Table 2. Raman analyses for gas and solids

Incl. type	Solid phases				Gas phases			
	Car	Gr	Rut	Nah	$\text{CO}_2$	$\text{CH}_4$	$\text{N}_2$	$\text{CO}_2/\text{CH}_4$
1	+	+	+	-	81	19	-	4.26
1	+	+	+	-	82	18	-	4.55
1	+	+	+	-	0	100	-	
1	+	+	+	-	0	100	-	
1	+	+	+	-	0	100	-	
1	+	+	+	-	0	100	-	
2	-	-	-	+	0	100	-	
2	-	-	-	+	0	100	-	
2	-	-	-	+	0	100	-	
2	-	-	-	+	89	11	-	8.10
2	-	-	-	+	18	82	-	0.22
2	-	-	-	+	0	100	-	
3	-	-	-	-	0	100	-	
3	-	-	-	-	98	2	-	49.00
3	-	-	-	-	94	6	-	15.60
3	-	-	-	-	95	5	-	19.00
3	-	-	-	-	15	58	27	0.26
4	-	-	-	-	0	100	-	
4	-	-	-	-	0	100	-	
4	-	-	-	-	0	99	1	
4	-	-	-	-	0	100	-	
4	-	-	-	-	0	99	1	
4	-	-	-	-	0	90	10	

Car-carbonate; Gr-graphite; Rut-rutile; Nah-nahcolite. + present; - absent.

Type 2 - these inclusions host daughter crystals of nahcolite (foto 2) identified by the peaks 463 and 1044  $\text{cm}^{-1}$  (figure 7). The gas phase contains usually higher  $\text{CH}_4$  and lower  $\text{CO}_2$  amounts (table 2).

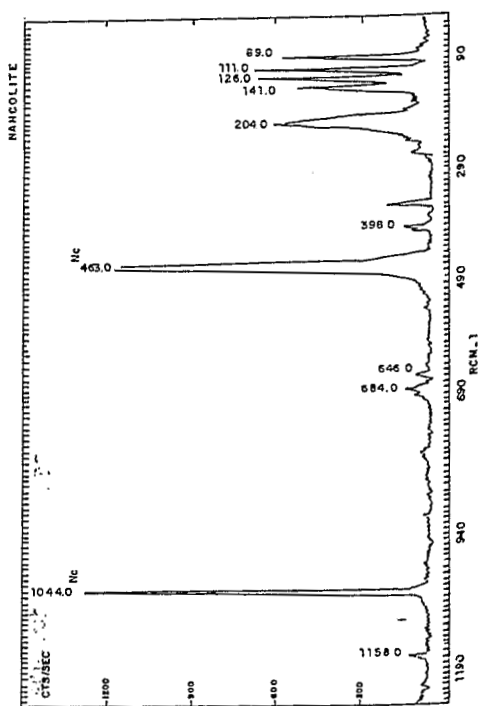


Fig. 7 Raman spectra of nahcolite

Type 3 - they contain vapour phases consisting mainly of  $\text{CO}_2$  with minor  $\text{CH}_4$  and  $\text{N}_2$  amounts (table 2).

Type 4 - the vapour phase consists essentially of  $\text{CH}_4$  with rare  $\text{N}_2$  (table 2).

Type 5 - in don't contain any detectable volatile, only  $\text{H}_2\text{O}$  (L and V).

### 5.3 Microthermometry data

The microthermometry has been done using a Chaixmeca apparatus with capability of temperatures between - 180°C and + 600°C.

Type 1 inclusions presented homogenization temperatures or fluid phases spanning from 300 to 420°C (figure 8). Only inclusions containing dominant  $\text{CO}_2$  displayed the homogenization temperature of  $\text{CO}_2$  at -6°C. Some dissolution of carbonates was observed during several heating runs.

Type 2 inclusions showed the homogenization temperature scattering in the 260-500°C range (figure 8). Dissolution of nahcolite was observed around 180°C.

Type 3 inclusions displayed homogenization temperatures varying in the 200 - 400°C range (figure 8). The melting temperatures of  $\text{CO}_2$  scattered from - 58 to about -70°C. The homogenization temperatures of the  $\text{CO}_2$  phases were extremely variable, but occur predominantly between + 10°C and + 11°C. The last melting of ice in presence of clathrate occurred between - 4 and - 7°C. The clathrate melting temperatures were observed between + 6 and + 16°C.

Type 4 inclusions displayed only homogenization temperatures in the vapour phase scattering in the 340-540°C range (figure 8).

Type 5 inclusions displayed homogenization temperatures in the liquid phase between 140 and 300°C (figure 8), and the last melting temperature of ice in the - 2°C to - 5°C range.

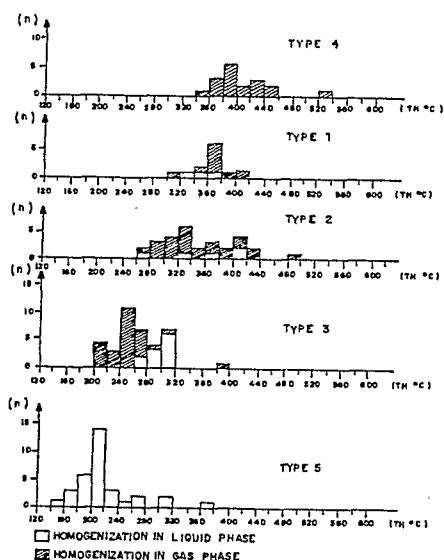


Fig. 8 Total homogenization temperatures of the main types fluid inclusions

## 6 CONCLUSIONS

In the auriferous quartz vein at the Pontal deposit the formation of type 1 inclusions synchronous with the trapping of oligoclase, actinolite/tremolite, biotite and native gold (solid inclusions in quartz), suggest a primary origin of these inclusions. Type 2 and 3 fluid inclusions rep-

resent early circulations of secondary fluids with variable  $\text{CO}_2/\text{CH}_4$  ratios (table 2). Type 4 inclusions represent high temperature and low density methane rich fluids, sometimes geometrically related to gold particles, although no convincing evidence supports the hypothesis of coeval type 1 and type 4 inclusions. Type 5 fluid inclusions correspond to late hydrothermal aqueous solutions.

From petrographic arguments, the trapping of type 1 multiphase and of the solid inclusions in quartz (including gold) occurred under the T-P conditions prevailing at the boundary between the greenschist and the amphibolite facies (biotite + actinolite + oligoclase stable). Referring to several authorities (Winkler, 1979; Turner and Verhoogen, 1960), T may be estimated to about 500-550°C, P being more difficult to constrain. However, type 1 inclusions with homogenization temperature of  $\text{CO}_2$  at -6°C can define the molar volume at about  $50\text{cm}^3/\text{mol}$  when the  $\text{CH}_4$  content is around 20% (Heyen et al., 1982). Using this value for formation temperatures (300-420°C and 500-550°C, the pressure can be estimated between 2 and 3 Kb, respectively (Holloway, 1981; figure 9).

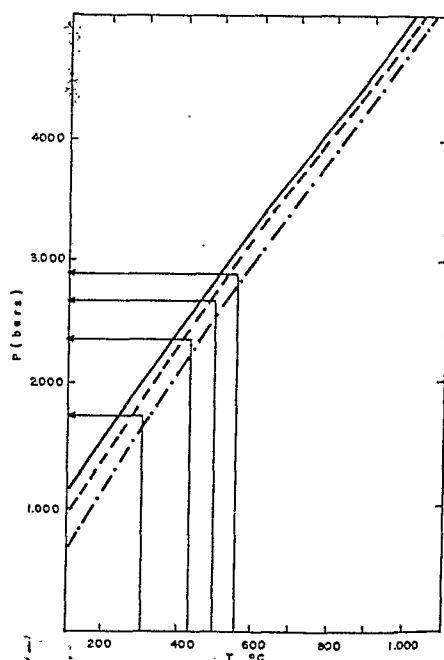


Fig. 9 Isochores of  $\text{CH}_4$  (full line),  $\text{CH}_4\text{-CO}_2$  (dashed line) and  $\text{CO}_2$  (dashed line-dot) for  $50\text{cm}^3/\text{mol}$

Most of type 1 fluid inclusions contain only detectable methane as a volatile component, but some inclusions (table 2) are dominated by  $\text{CO}_2$ . At  $500^\circ\text{C}$ , with the ratio  $\text{CO}_2/\text{CH}_4 = 4$  and in equilibrium with graphite,  $f_{\text{O}_2}$  plots slightly over the QFM buffer, for the estimated pressure (Kreulen, 1987; point A in figure 10). Although for inclusions without detectable  $\text{CO}_2$ ,  $f_{\text{O}_2}$  is evidently lower but cannot be estimated, the plots were made for  $\text{CO}_2/\text{CH}_4 = 1/99$  (point B in figure 10). These variations of  $f_{\text{O}_2}$  at the time of primary fluid inclusion trapping, resulting from precipitation of the graphite phase (Dubessy, 1984), may have triggered gold precipitation through destabilization of  $\text{Au}(\text{HS})_2^-$  complex (Touray, 1987; Shenberger et al., 1989).

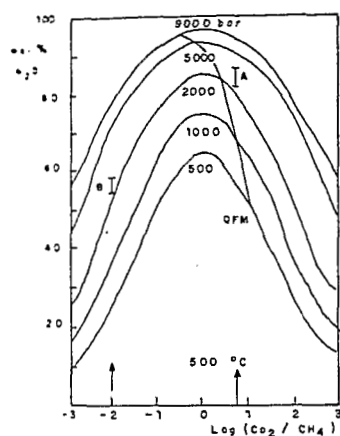


Fig. 10 Relation between  $\log (\text{CO}_2/\text{CH}_4)$  and mol %  $\text{H}_2\text{O}$  in graphite buffered fluids

Finally, the Pontal auriferous quartz vein may be described as high temperature metamorphic deposit (Movarek et al., 1987), formed under variable oxygen fugacity, with redox conditions ranging from QFM buffer to lower values. A major unsolved problem is the origin of the carbon-bearing fluids: because the usual assumption of a source from graphitic shales may hardly be invoked, in view of the lacking of such sediments in the basement, some deep crustal (or mantle) source appears more probable.

Similarly, the classical hypothesis of a gold source within local ultrabasic rocks seems unlikely, and some deep source has to be invoked.

## REFERENCES

- Costa, J.B.S. & Hasufi, Y. 1988. Aspectos do lineamento transbrasileiro na região de Porto Nacional - Natividade-GO. Abstracts do XXXV Congresso Brasileiro de Geologia. Belem (PA): 182.
- Dubessy, J. 1984. Simulation des équilibres chimiques dans les systèmes C-O-H. Conséquences méthodologiques pour les inclusions fluides. *Bull. Mineral.*, Vol. 107: 156-168.
- Guilhemou, N.; Santos, M.M.; Touray, J.C.; Beny, C. & Dardenne, M.A. 1989. Multiphase methane-rich fluid inclusions in gold bearing quartz as illustrated at Pontal (Goiás, Brazil). *Proceedings of Gold'89*, Toulouse, France.
- Hasufi, Y. & Haralyi, N.L.E. 1985. A megatrusturação de Goiás. 2º Simpósio de Geologia do Centro-Oeste, Sociedade Brasileira de Geologia: 120-144.
- Heyen, G.; Ramboz, C. & Dubessy, J. 1982. Simulation des équilibres de phases dans le système  $\text{CO}_2\text{-CH}_4$  endessous de  $50^\circ\text{C}$  et de 100 bar. *C.R. Acad. Sc.Fr.*, Vol. 294: 203-206.
- Holloway, J.R. 1981. Compositions and volumes of super-critical fluids in the Earth's crust. In: *Short course in fluid inclusions - Applications to petrology* (L.B. Hollister and M.L. Grawford, eds), cap. 2: 13-38.
- Kreulen, R. 1987. Thermodynamic calculations of the C-O-H system applied to fluid inclusions: are fluid inclusions unbiased samples of ancient fluids? *Chemical Geology*, V. 61: 59-64.
- Movarek, P. & Pouba, Z. 1987. Precambrian and Phanerozoic history of gold mineralization in the Bhoemian massif. *Econ. Geol.* V. 82: 2098-2114.
- Shobbenhaus, C.F. 1975. Carta geológica do Brasil ao milionésimo. Brasília. DNPM; 13-57, 74-85.
- Shenberger, D.M. & Barnes, H.L. 1989. Solubility of gold in aqueous sulfide solutions from  $150^\circ\text{C}$  to  $350^\circ\text{C}$ . *Geochim. Cosmochim. Acta* 53: 269-278.
- Touray, J.C. 1987. Transport et dépôt de l'or dans fluides de la croûte continentale, l'apport de études d'inclusions fluides, *Chron. de la Rech. Min.* 484: 43-53.
- Turner, F.J. & Verhoogen, J. 1960. *Igneous and Metamorphic Petrology*, 2nd edit., McGraw-Hill Book Company, New York.
- Winkler, H.G.F. 1979. *Petrogenesis of metamorphic rocks*. Ed. 5. New York, Springer-Verlag, 348p.

# BRAZIL GOLD '91

E.A.Ladeira

Editor

The Economics Geology Geochemistry and  
Genesis of Gold Deposits



O.R.S.T.O.M. Fonds Documentai  
N° : 34.850-06-1  
Cpte : B M